# Design and Fabrication of Stainless-Steel Battery Case with Integrated Internal Cooling Channels Using Binder Jetting Additive Manufacturing

Henil P. Patel[1] and Amir A. Yahyaeian[2]
*Embry-Riddle Aeronautical University, Daytona Beach, Florida, 32114, USA*

Yue Zhou[3]
*Embry-Riddle Aeronautical University, Daytona Beach, Florida, 32114, USA*

**Rechargeable lithium-ion (Li-ion) batteries are widely used in aircraft and aerospace applications due to their high energy density and compact design. As these batteries generate significant heat during charge-discharge cycles, effective thermal management is essential to prevent performance degradation and potential thermal runaway. One promising approach is optimizing internal cooling channel geometries within battery cooling cases to enhance heat dissipation. Despite the importance of thermal management, the influence of cooling channel geometry on heat transfer efficiency remains underexplored. This study focuses on the design optimization and computational evaluation of cooling channel geometries. Three designs, including circular, dented, and curved are analyzed using Computational Fluid Dynamics (CFD) to assess temperature distribution, velocity profiles, and pressure drop. Binder jetting additive manufacturing is employed to fabricate stainless steel battery case prototypes, which are further analyzed for microhardness and surface roughness. Results indicate that curved channels exhibit superior cooling performance, with an outlet temperature of 17.0°C, a maximum velocity of 20.3 mm/s, and a net heat transfer rate of 1148 W. The final prototype demonstrates an average microhardness of 148 HV and surface roughness of 26 µm, highlighting the feasibility of optimized cooling geometries for enhanced thermal management in Li-ion batteries.**

## I. Nomenclature

| | | |
|---|---|---|
| *AM* | = | additive manufacturing |
| *BJ* | = | binder-jetting |
| *Li-ion* | = | lithium ion |
| *CFD* | = | computational fluid dynamics |
| *CAD* | = | computer aided design |
| c | = | chord |
| d*t* | = | time step |
| *Fx* | = | *X* component of the resultant pressure force acting on the vehicle |
| *Fy* | = | *Y* component of the resultant pressure force acting on the vehicle |
| *f, g* | = | generic functions |
| *h* | = | height |
| *i* | = | time index during navigation |
| *j* | = | waypoint index |
| *K* | = | trailing-edge (TE) nondimensional angular deflection rate |

## II. Introduction

Rechargeable lithium-ion (Li-ion) batteries are widely used in the aerospace and automotive industry due to reduced mass and size, ease of production and testing, and lowered manufacturing costs compared to conventional

[1] Undergraduate Student, Aerospace Engineering Department, and University Student.
[2] Graduate Student, Aerospace Engineering Department, and University Student.
[3] Assistant Professor, Aerospace Engineering Department.

nickel-based and aqueous battery systems [1, 3]. In the Mars Surveyor program, NASA equipped its first Martian lander with two 9 kg Li-ion batteries for a one-year cruise period [2]. The Boeing 787 Dreamliner, for instance, utilizes two Li-ion batteries to start auxiliary power units and serve as a backup in case of electronic system failures [6]. Despite their exceptional physical and chemical properties, Li-ion batteries inevitably generate significant heat during charge and discharge cycles due to electrochemical reactions [7]. If the heat is not managed well, the overheating of the battery cells could increase the risk of a thermal runaway, degrade the battery components, and shorten the battery life. In 2013, two cases of battery fire on the Boeing 787 Dreamliner led to the grounding of the entire fleet for nearly four months. The primary reason for battery fire, as reported by the investigating authorities, was a short circuit in one of the battery cells, which resulted in a thermal runaway i.e., damaging and causing fire in adjacent cells [5].

As a response to battery fire incidents, Boeing implemented a passive cooling approach by enclosing Li-ion batteries in a metallic fire-resistant casing and integrating a venting system to expel smoke in the event of a fire [8]. While passive cooling provides basic thermal protection, direct liquid cooling systems have demonstrated superior heat dissipation and thermal efficiency [9, 10]. To further enhance thermal management, battery cases with integrated internal cooling channels can be designed and fabricated to more effectively regulate heat during peak battery operation. Several studies have investigated the effects of cooling channels within thermal management systems on the heat dissipation and temperature uniformity. Notably, Zhao et al. [3] introduced a hybrid cooling approach that integrates direct liquid cooling with forced air cooling. Their study demonstrated that increasing the number of cooling channels had a negligible effect on temperature regulation within battery cells; however, maintaining a constant mass flow rate while adding additional channels reduced energy consumption and improved overall cooling efficiency. Similarly, Xu et al. [6] analyzed the thermal performance of different cooling channel configurations by comparing serpentine and U-shaped designs for Li-ion batteries. Their findings indicated that the serpentine channel exhibited superior cooling efficiency, with an optimized design reducing the maximum temperature difference (MTD) within the battery pack by 7.46%.

In addition to experimental studies, numerical modeling plays a vital role in predicting the thermal performance of cooling systems in battery packs. By simulating various physical phenomena such as heat generation, distribution, and dissipation, numerical models offer valuable insights for optimizing battery efficiency, safety, and longevity. For instance, Duan et al. [7] performed a numerical analysis to investigate the impact of channel size and inlet temperature on the thermal behavior of discharging Li-ion battery cells. Their findings revealed that larger cooling channel sizes reduced the energy consumption of the cooling system, while higher inlet flow rates enhanced heat transfer performance. In another study, Quan [8] proposed a liquid-cooled thermal management solution using a single cooling plate channel attached to the battery pack. It was shown that increasing the width and thickness of cooling channels effectively reduced maximum temperature distribution within the battery pack, thereby enhancing cooling efficiency. Egab and Oudah [9] developed an air-based cooling system that incorporated perforated fins in various shapes (e.g., circular, elliptical, and cylindrical) within the cooling channels. Their results demonstrated that the inclusion of perforated heat sinks and dimples, especially in elliptical configurations, significantly reduced the temperature of the battery pack by enhancing air convection.

Cooling channels often feature complex geometries, but conventional manufacturing technologies face intrinsic limitations in achieving such complexity. Compared to integrated manufacturing, assembling multiple thermal components increases the risk of common mode failures [11]. In recent years, additive manufacturing (AM) has emerged as a promising solution for fabricating complex-shaped metallic components with reduced lead time and material waste [12]. In particular, Binder Jetting (BJ), an AM technique that offers distinct advantages for manufacturing intricate cooling channels within battery cases. In BJ, a liquid binder is selectively deposited onto layers of metal powder, forming a "green part" that is subsequently sintered to achieve the final structure [13]. This technique provides several key benefits, including lower machine costs, compatibility with a wide range of materials, and high scalability [13]. In addition, BJ minimizes residual stresses by eliminating the use of high-energy beams, thereby reducing the risk of warping or distortion [14]. The powder bed setup further enhances manufacturing efficiency by eliminating the need for support structures, facilitating the production of overhanging features [14].

Recent studies have extensively examined the effects of particle characteristics, process parameters, and post-processing conditions on the porosity, microstructure, and mechanical performance of metallic parts fabricated using BJ additive manufacturing [15-17]. However, research on BJ for complex internal structures, particularly in thermal management applications, remains limited. Addressing this gap is crucial for advancing high-performance cooling solutions in aerospace, automotive, and energy storage systems. In this work, stainless steel (SS) 420 was selected to fabricate scaled-down battery case prototypes with integrated cooling channels using BJ. Process parameters and sintering profiles were optimized to improve porosity and microhardness. Computational Fluid Dynamics (CFD) simulations were conducted to evaluate temperature profile, pressure drop, outlet velocity, and heat transfer efficiency. Further, by incorporating the effects of surface roughness and porosity inherent to BJ-processed parts into the

simulations, computational model was re-iterated. This research aims to establish fundamental relationships between geometry, manufacturing processes, and thermal performance in BJ-fabricated battery case prototypes. By improving the understanding of how cooling channel design influence heat dissipation, these findings will contribute to the development of next-generation metallic thermal management systems. Ultimately, this work lays the foundation for innovative cooling solutions in practical applications, where efficient thermal regulation is critical for safety and performance.

## III. Methodology

The following sections details the research methodology adopted to conduct this research.

### A. Design of Cooling Channels

The distribution and geometry of cooling channels significantly influence the heat transfer performance of a battery case, as they directly affect the fluid flow field and temperature distribution within the channels. In this study, three channel geometries (circular, bent, and curved) were designed within battery case prototypes and analyzed as shown in Figure 1. Firstly, the circular channel was selected as the baseline design due to its widespread use in heat exchanger applications [19]. Its simple geometry allows for uniform coolant flow with minimal disturbance, making it an effective reference for comparison. Additionally, circular channels naturally minimize pressure drop, which is advantageous for maintaining efficient fluid flow without excessive power requirements. However, one limitation of this design is its restricted surface area for heat exchange, which can reduce overall thermal dissipation efficiency compared to more complex geometries. Secondly, the dented channel was introduced to enhance surface area and promote turbulence, both of which contribute to improved convective heat transfer. By incorporating localized indentations along the channel walls, this design is expected to increase the contact interface between the coolant and the channel surface, leading to more effective heat dissipation. Additionally, the dents could induce localized turbulence, which helps to disrupt thermal boundary layers, further optimizing convective cooling. Finally, the curved channel was designed to optimize fluid acceleration and mixing by introducing flow redirection along the channel path. This geometry generates secondary vortices, which enhance fluid mixing and thermal diffusion, leading to more effective convective heat transfer. The trade-off could be a higher pressure drop, as the curvature forces the fluid to navigate more abrupt directional changes, increasing flow resistance compared to both the circular and dented channels.

These geometries were modeled using CATIA v5 software. The prototype battery case, depicted in Figure 1(a), consists of a hollow cubic shell with multiple channels integrated into its walls. To simplify the manufacturing and simulation, the prototype dimensions were scaled down to 40 × 40 × 40 mm with a uniform wall thickness of 6 mm. The specific shapes and dimensions of each channel are illustrated in Figure 1(b-d). Regardless of shape, all channels maintain a constant cross-sectional area along their length, ensuring a uniform volume flow.

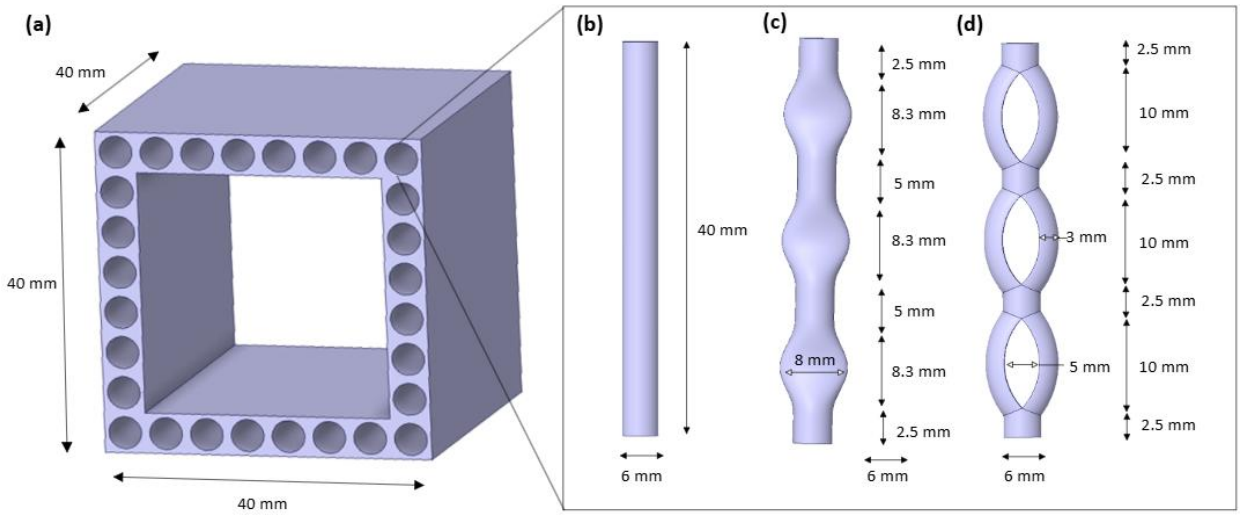


**Fig. 1 (a) Design of the battery case with internal cooling channels and; dimensions of (b) circular, (c) bent, and (d) curved cooling channels.**

**B. CFD Modelling**

ANSYS Fluent software was used to simulate the fluid dynamics at the outlet of the channels. To improve simulation efficiency, the following assumptions were made:

1. The battery or heat source was assumed to radiate heat uniformly along its entire length, leading to a
2. constant wall temperature equal to the temperature of the batteries inside the case.
3. Conduction, convection, and radiation within the battery pack were neglected, and the battery's heat capacity was assumed to remain constant throughout the heat transfer process [6].
4. A no-slip condition was assumed between the wall and the fluid, with radiation heat transfer considered at the wall.
5. Steady-state flow was assumed.

After designing the prototype battery case in CATIA v5, the models were exported to ANSYS SpaceClaim to extract the fluid volume from the cooling channels using the "Volume Extract" feature. This step enabled finer meshing of the fluid body compared to the battery case walls for more accurate fluid flow results. Once the fluid volume was extracted, named selections were made for the inlets, outlets, battery case walls, and fluid body, preparing the models for meshing. The models were then transferred to the "Watertight Workflow Geometry" workbench in Fluent. To mesh the model, the double precision tab was activated and meshing and solver processes were set to 4. The meshing procedure involved adding "Local Sizing" to the inlet and outlet with a target mesh size of 0.5 mm, generating a surface mesh with a minimum size of 0.1 mm and a maximum size of 1 mm. Boundary zones were separated by a maximum angle of 18°, and the surface mesh had a maximum skewness of 0.44, which is acceptable in ANSYS Fluent. A non-conformal meshing process was applied. Boundary conditions were set with the inlet as a velocity inlet, the outlet as a pressure outlet, and the exterior fluid wall as a wall. The model geometry was defined as fluid, and appropriate boundary layers were specified. The volume mesh was generated as "polyhedral" with a maximum cell length of 0.65 mm. Figure 5 shows the cross-sectional view of the mesh, consisting of 8 cell zones, 101,263 cells, and a minimum orthogonal quality of 0.20. After meshing, a final mesh check was performed to ensure the model was error-free before transferring it to Fluent Solvent for analysis.

In the model, a pressure-based solvent type was adopted, and a steady state flow was assumed. The effect of gravity was also considered in the simulation, with the gravitation constant being $g = 9.81\ m/s$. he energy equation was activated, and laminar flow was assumed based on the Reynolds number, as calculated in Equation (1). Cell zone conditions were defined, and the appropriate materials were assigned: water for the internal fluid and stainless steel for the battery case walls.

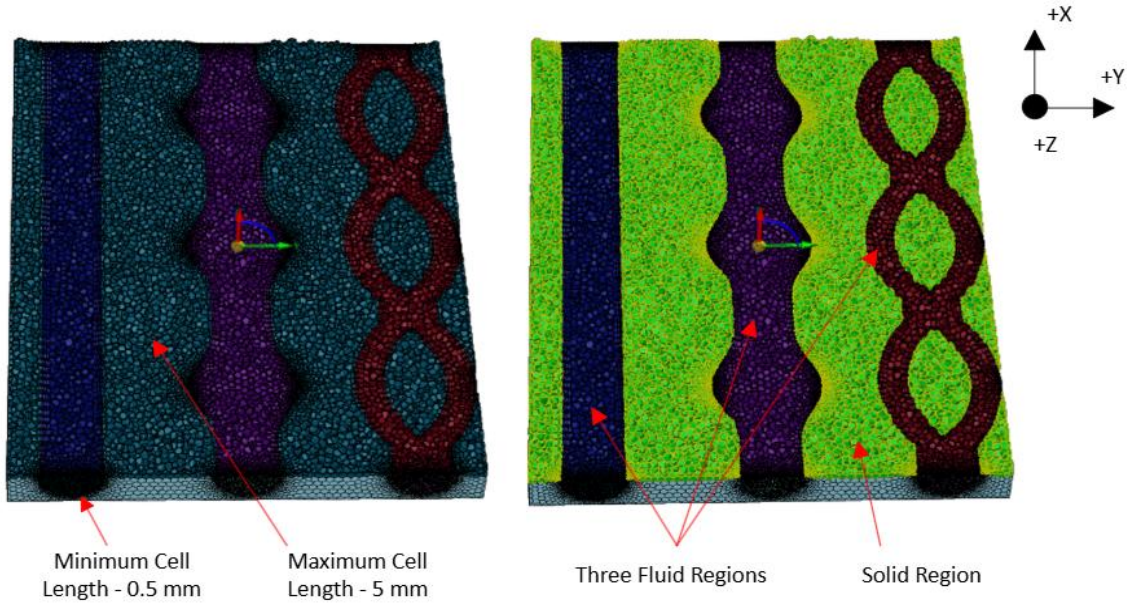


**Fig. 2 Visual representation of the volume mesh for the fluid body through circular elliptical channe**l.

$$Re = \frac{\rho V d}{\mu} \tag{1}$$

where $\rho$ is the density of water, $V$ is the velocity of the water at the inlet, $d$ is the hydraulic diameter of the pipe, and $\mu$ is the dynamic viscosity of water. The Reynolds number was estimated to be 67.29, indicating a laminar flow.

The heat dissipated by the battery to the steel case is transferred to the fluid by convection; this quantity was modeled using Newton's law of cooling. The amount of heat dissipated by the movement of fluid is given by the following equation, where q is the rate of heat transfer ($W/m^2$), h is the convection heat transfer coefficient (W/$m^2.K$), $T_b$ is the body or surface temperature (K), and $T_f$ is the temperature of the fluid (K) [11].

$$q = h(T_s - T_a) \tag{2}$$

The temperature distribution at the outlet of the channel is determined by the energy equation, as shown below [6].

$$\rho \frac{\partial T}{\partial t} + \nabla.\left(\rho \vec{V} T\right) = \nabla.\left(\frac{k}{c} \nabla T\right) \tag{3}$$

where $\rho, k, c$ represent density, thermal conductivity, and specific heat capacity of the coolant (liquid water). Continuity equation of the coolant is described below [6]. The mass and linear momentum balance of which are solved by partial differential equations (4) and (5) to obtain the velocity fields:

$$\nabla \cdot \left(\rho \vec{V}\right) = 0 \tag{4}$$

$$\rho \frac{\partial \vec{V}}{\partial \mathrm{x}} + \rho \vec{V} \cdot \nabla v = -\nabla p + \nabla \cdot \mu \left(\nabla \vec{V} + \left(\nabla \vec{V}\right)^T\right) + \rho \vec{g} \tag{5}$$

**Table 1:** Physical parameters for materials used in this simulation are given in the table below [10]:

| **Material** | **Density** $(kg/m^3)$ | **Specific Heat** $(J/kg.K)$ | **Thermal Conductivity** $(W/m.K)$ | **Viscosity** $(kg/m.s)$ |
|---|---|---|---|---|
| **Water** | 998.2 | 4182 | 0.6 | 0.001003 |
| **Stainless-Steel** | 8030 | 502.48 | 16.27 | - |
| **Battery** | 2500 | 1000 | 3 | - |

The cell zone for the structure was defined as the fluid body, with water as the material type. Boundary conditions were set at the inlet, where the water velocity was 0.01 m/s and the temperature was 10°C. Thermal convection through the walls into the fluid was established for the heat source. The battery, assumed to radiate heat uniformly along its length, was modeled at a constant wall temperature equal to the temperature of the batteries inside the case, set at 40°C (assuming the battery was in a discharging state). The wall thickness was 0.5 mm. Further assumptions, based on similar studies, included: the battery was isotropic, conduction, convection, and radiation inside the battery pack were neglected, and the battery's heat capacity remained constant throughout the heat transfer process [6]. A no-slip condition was applied between the wall and the fluid body, and radiation heat transfer was ignored. The hybrid initialization method was used for the flow simulation, which was run for 100 iterations. The results were presented as contours and pathlines throughout the fluid body structure.

### C. Binder Jetting Additive Manufacturing

The feedstock for BJ process is SS 420 particles with a diameter range of 30 microns. Figure 2 presents a schematic diagram illustrating the setup and process of the BJ additive manufacturing system. The BJ process begins with slicing the 3D CAD models into 2D layers of a specified thickness using proprietary software integrated with the BJ machine. The printing process starts with the deposition of metallic powder onto the build platform from a hopper. A roller with controlled rotational and translational speeds evenly spreads the powder across the platform to form a uniform layer. An inkjet printhead moves along the X and Y axes, depositing microscopic droplets of binder onto designated areas of each layer. The binder adheres to the powder particles through capillary forces, forming a rudimentary structure. After binder application, an electrical heater dries the layer and maintains uniform temperature to prevent warping. This process repeats with the piston lowering along the Z-axis after each layer, gradually building the 3D structure. The binder creates inter-particle bonds, forming a "green part," as shown in Figure 3(a). Table 1 summarizes the optimized process parameters.

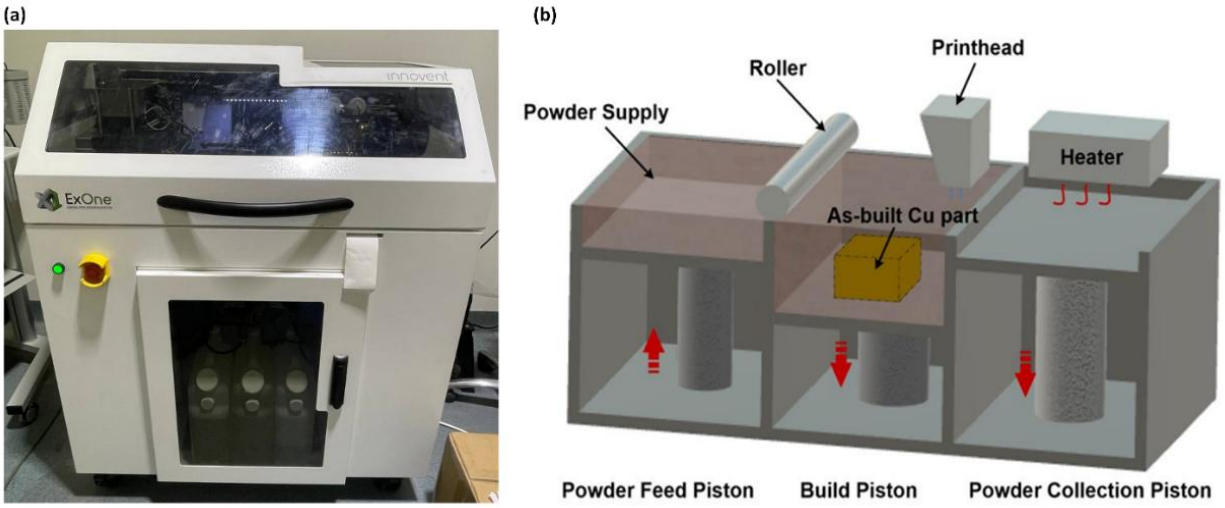


**Fig. 3 (a) Illustration of ExOne innovent+ binder jetting 3D printer used for fabricating battery cases (b) schematic diagram of metal binder jetting process.**

**Table 2: Optimized process parameters for binder jetting**

| Process parameters | Values |
|---|---|
| Binder saturation ratio (%) | 100 |
| Layer thickness (μm) | 20 |
| Powder bed temperature (°C) | 60 |
| Drying time (s) | 12 |
| Recoating speed (mm/s) | 25 |
| Roller transverse speed (mm/s) | 5 |
| Roller rotational speed (rpm) | 700 |

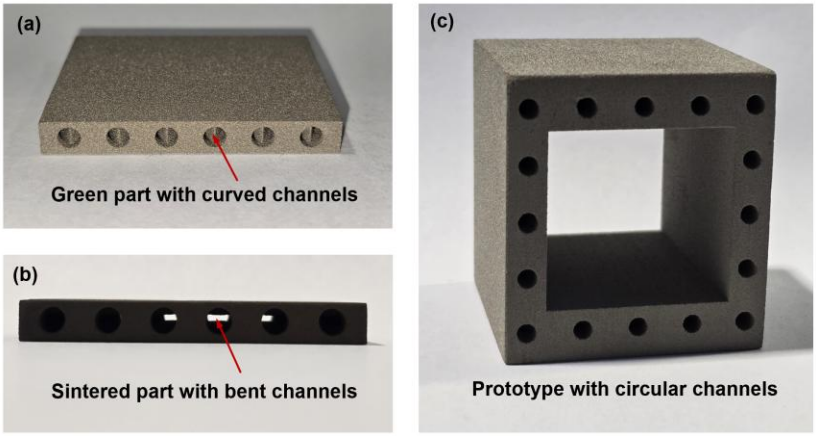


**Fig. 4 Representative samples: (a) green part, (b) sintered part, and (c) prototype with various cooling channels.**

After printing, the green part was cured at 200°C to solidify the binder and improve structural integrity for handling and post-processing. Excess powder was removed through "depowdering" using a soft brush or pressurized air, with reclaimed powder often reused to enhance material efficiency. The as-built parts then underwent "debinding," where the binder was removed thermally or chemically to prepare for sintering. In the sintering phase, high temperatures induced atomic diffusion, bonding powder particles to achieve the desired density and mechanical properties. Figure 4 outlines the optimized sintering profile and detailing key parameters.

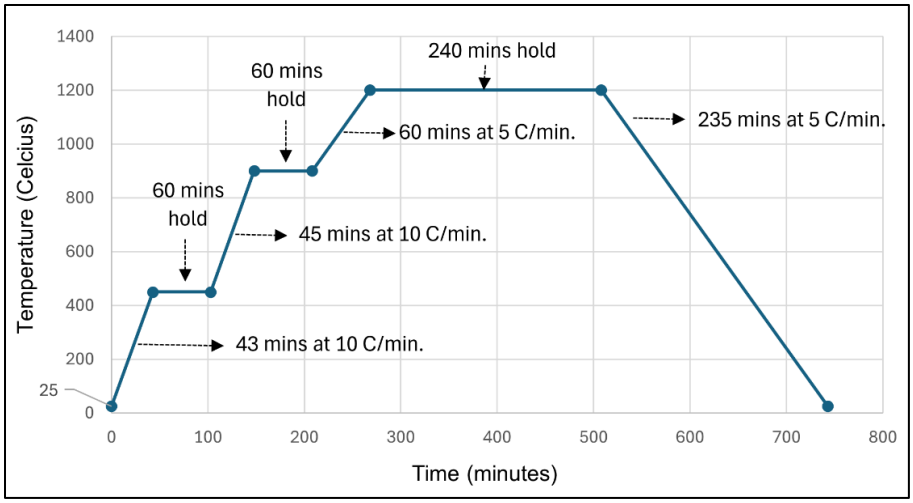


**Fig. 5 Optimized sintering profile used for as-built SS 420 parts**.

## IV. Results & Discussion

The design, distribution, and geometry of the cooling channels significantly influences the heat transfer performance of the battery case. The heat transfer can be analyzed by measuring the fluid's temperature and velocity gradient and pressure drop as it moves through the cooling channels. These physical parameters were measured using simulations performed in ANSYS Fluent. Figure 6 show below indicates the velocity and pressure variations of the coolant as it passes through the different cooling channels.

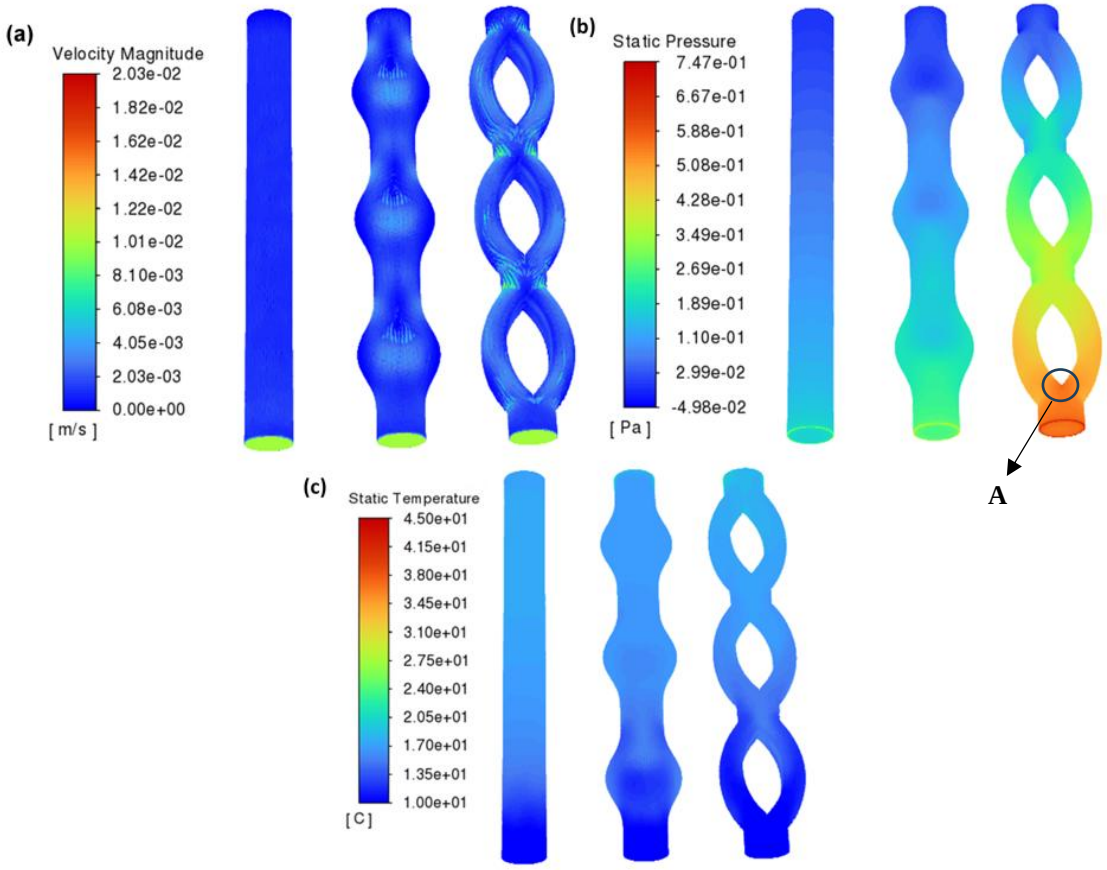


**Fig. 6 (a) Velocity pathlines of the fluid body through different channels. (b) pressure drop in the cooling channels. (c) Thermal distribution inside the channels.**

From Figure 6, Figure 4 illustrates the pressure distribution across the three cooling channels, revealing the hydrodynamic resistance introduced by each geometry. As expected, the curved channel experiences the highest pressure drop, resulting from complex flow paths and induced secondary vortices. The higher resistance slows down fluid movement, improving heat absorption but increasing pumping power requirements. The dented channel exhibits a moderate pressure drop, as the localized surface indentations introduce flow disruptions without excessive resistance. This makes it a compromise between enhanced convective cooling and flow efficiency. Meanwhile, the circular channel shows the lowest pressure drop, as it maintains a straight, unobstructed flow path. However, its low hydrodynamic resistance comes at the cost of reduced thermal dissipation, reinforcing the trade-off between pressure loss and heat transfer efficiency. These results highlight that while turbulence-induced heat transfer can be beneficial, excessive pressure drop must be minimized to ensure efficient coolant circulation without excessive energy consumption. The curved channel, while thermally efficient, may not be the most practical choice in applications where energy efficiency is a priority. As seen in part (b) of the Figure 6, there is a back-pressure zone generated, indicated as pt. A, which disrupts the flow of the coolant by generating a turbulent wake and increases the pump load of the sideways channel, thereby leading to higher energy consumption.

The velocity distribution of the coolant was analyzed to assess the flow characteristics of each cooling channel, as depicted in Figure 6 (a). The circular channel exhibits a nearly uniform velocity profile, meaning the coolant flows smoothly with minimal disturbances. However, this also indicates lower fluid-wall interaction, limiting its convective heat transfer potential. In contrast, the dented channel exhibits localized velocity fluctuations along its surface deformations, promoting boundary layer disruption and increased turbulence-enhanced cooling. This results in higher heat absorption rates compared to the circular channel, while maintaining a relatively stable flow pattern. The curved channel demonstrates the most pronounced velocity variations, with increased flow acceleration and secondary vortices along its bends. These effects improve coolant mixing and convective heat transfer efficiency, explaining why the curved channel achieves the highest outlet temperature. However, this higher velocity also contributes to increased flow resistance and energy consumption, which is further analyzed in the pressure drop evaluation.

.

**Table 3: Physical parameters at inlet and outlet of the different cooling channels.**

| Channel Shapes | Inlet Temperature (℃) | Inlet Velocity ($\boldsymbol{mm/s}$) | Outlet Velocity ($\boldsymbol{mm/s}$) | Pressure Drop (Pa) | Outlet Temperature (℃) |
|---|---|---|---|---|---|
| Circular | 10 ℃ | 10.0 $mm/s$ | 14.2 $mm/s$ | 0.189 Pa | 17.0 ℃ |
| Bent | 10 ℃ | 10.0 $mm/s$ | 18.2 $mm/s$ | 0.349 Pa | 24.0 ℃ |
| Curved | 10 ℃ | 10.0 $mm/s$ | 20.3 $mm/s$ | 0.667 Pa | 27.5 ℃ |

Table 3 indicates the inlet and outlet parameters of the coolant for each channel shape. Sideways channel has the maximum outlet temperature and velocity of 27.5 ℃ and 20.3 $mm/s$ respectively. The significant rise in temperature for the sideways channel is due to increased surface contact of the fluid. The variation in heat transfer area significantly impacts the final temperature performance in three different shaped channels because the heat transfer area directly affects the effectiveness of convective heat transfer [18]. Larger or more optimized heat transfer areas enhance the interaction between the fluid and the channel surface, improving heat dissipation and reducing the thermal resistance to convection. Conversely, smaller or less effective areas limit heat transfer, resulting in lower final temperatures like the circular channel. Therefore, differences in channel geometry and surface area can lead to substantial variations in temperature performance, even under similar flow and thermal conditions. The shape and distribution of the sideways channel allows for greater fluid to come in contact with the battery case walls at a greater temperature.

Figure 8 show below indicates the sample prototypes fabricated using binder jetting additive manufacturing for all three channel shapes, showcasing complex internal structures printed by the 3D-printer. After fabrication, the parts were tested for roughness constant using a profilometer. Figure 8 shown below illustrates the profilometer results for sintered battery case prototype. The average roughness of the prototype in the direction of the fluid flow field in is 21.9μm.

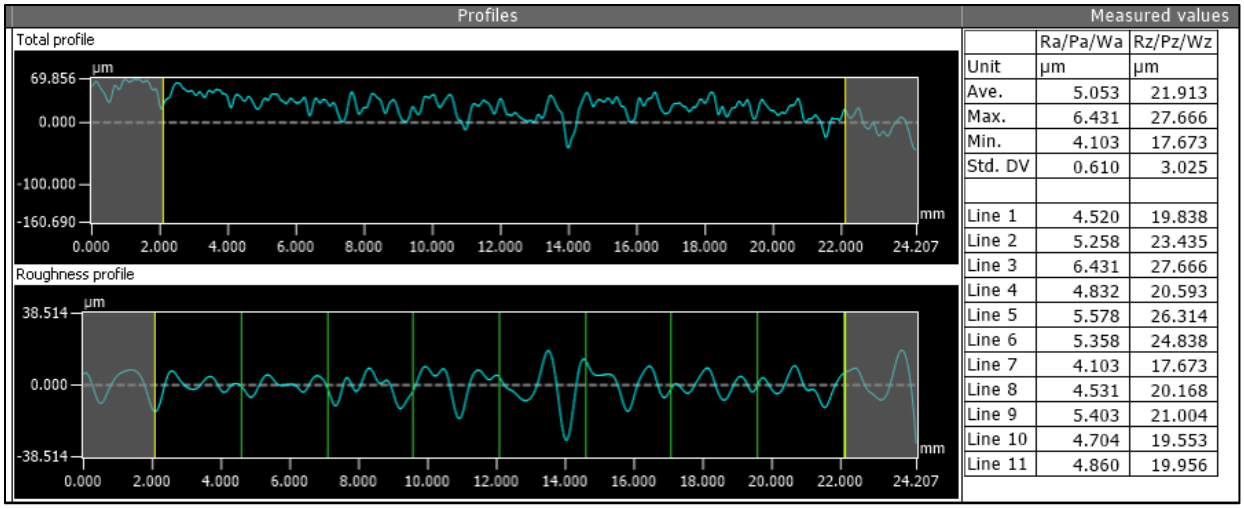


| | Ra/Pa/Wa | Rz/Pz/Wz |
|---|---|---|
| Unit | µm | µm |
| Ave. | 5.053 | 21.913 |
| Max. | 6.431 | 27.666 |
| Min. | 4.103 | 17.673 |
| Std. DV | 0.610 | 3.025 |
| | | |
| Line 1 | 4.520 | 19.838 |
| Line 2 | 5.258 | 23.435 |
| Line 3 | 6.431 | 27.666 |
| Line 4 | 4.832 | 20.593 |
| Line 5 | 5.578 | 26.314 |
| Line 6 | 5.358 | 24.838 |
| Line 7 | 4.103 | 17.673 |
| Line 8 | 4.531 | 20.168 |
| Line 9 | 5.403 | 21.004 |
| Line 10 | 4.704 | 19.553 |
| Line 11 | 4.860 | 19.956 |

**Fig. 7 Profilometer results of measuring roughness constant of the sintered battery case prototype.**

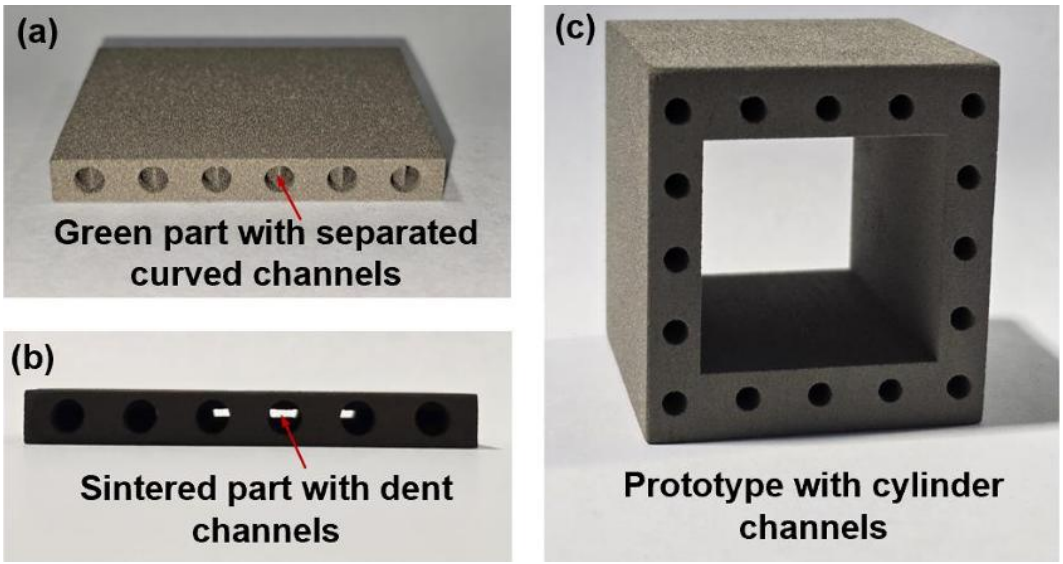


**Fig. 8 Representative samples: (a) sample case wall with sideways channels (green part), (b) case wall with bent channel (sintered part), and (c) case prototype with various sideways cooling channels (green part).**

The microhardness was tested on the external surfaces of sintered parts. The microhardness of sintered samples was in the range of 130-260 HV. From Figure 9, several locations demonstrate lower microhardness, which can be attributed to the presence of interior defects such as pores, inclusions, or incomplete sintering that create 7 weak points in the material structure. These defects reduce the overall load-bearing capacity during testing, leading to localized reductions in hardness. The observed variation in microhardness across different regions of the sintered steel parts indicates a heterogeneous distribution of density and microstructural features. Regions with higher microhardness values suggest a more homogeneous microstructure, possibly due to better particle bonding and fewer voids. In contrast, areas with lower microhardness may have experienced less uniform compaction or sintering, resulting in increased porosity or larger grain sizes, which can negatively affect the mechanical properties.

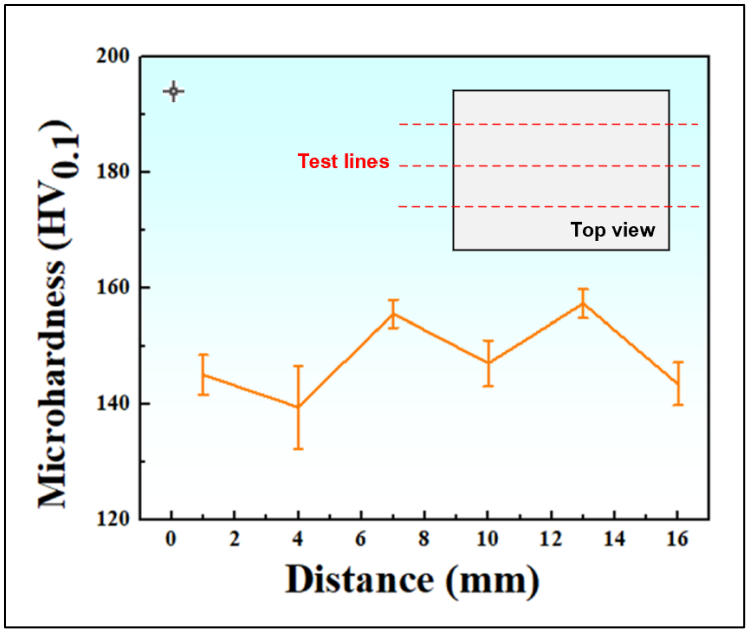


**Fig. 9 Microhardness profile of the sintered battery case prototype in X-Y plane.**

## V. Conclusion

A thermal management device or a battery case with internal integrated cooling channels was designed and fabricated to provide active cooling to Li-ion batteries. Three channel shapes were tested for CFD analysis in ANSYS Fluent namely circular, bent, and curved. It was found that the fluid flowing through the curved channel had the maximum outlet temperature of 27.5 ℃, as compared to 24.0 ℃ and 17.0 ℃ for bent and circular channels respectively. This indicates that higher coolant amount comes in contact with the battery case, improving the thermal efficiency of the channel shape. Further, the curved channels also had the maximum outlet velocity and pressure drop of 20.3 mm/s and 0.667 Pa respectively. Larger pressure drop and higher inlet pressure due to curved channel shape indicates the formation frontal vortices, which provides resistance to the coolant flow and increases its surface contact, thereby making the curved shape a thermally superior and efficient channel design. Finally, a faster outlet velocity of the curved channels indicates reduced viscosity and higher heat absorbance. Since the performance of bent channel is superior to the circular channel, it can be concluded that shape modifications of the cooling channels have a significant impact on the thermal efficiency of the battery case. The pressure, temperature, and velocity variations were also analyzed along the length of the channels, and the variations were studied. Chanes in shape along the length of the cooling duct results in better heat transfer in the fluid. Additionally, the formation of turbulent wakes inside the coolant profile results in higher convection heat transfer. However, the power consumption will be higher by pumping the coolant through the channel with different shapes. For having equal mass flow rate through all three channels, the curved channel will consume maximum power than the bent channel; power consumption for the circular channel would be minimum. The average roughness constant for the manufactured battery cases was measured to be 21.9µm, while the average microhardness was 148 HV. These parameters resulted in lower pressure drop and outlet velocity when considered in simulation. However, the channel performance remained the same: the curved channels result in the highest cooling effect.

## References

[1] Marsh, R. A., et al. “Li ion batteries for aerospace applications.” Journal of Power Sources, no. 2001, 30 Dec. 2001, pp. 25–27, https://doi.org/https://doi.org/10.1016/S0378-7753(01)00584-5.

[2] Surampudi, Surya Kiran, and B. V. Ratnakumar. “Lithium-ion batteries for aerospace.” IEEE Aerospace and Electronic Systems, no. 2004, Feb. 2004, pp. 1–8, https://doi.org/10.1109/MAES.2004.1263988.

[3] Clarke, Matthew, and Juan J. Alonso. “Lithium–ion battery modeling for Aerospace Applications.” Journal of Aircraft, vol. 58, no. 6, Nov. 2021, pp. 1323–1335, https://doi.org/10.2514/1.c036209.

[4] Hansson, Niklas, et al. “Environmental Impacts of Aerospace Batteries.” Boeing Technical Journal, no. 2018, 2018,https://doi.org/https://www.boeing.com/content/dam/boeing/boeingdotcom/features/innovation-quarterly/aug2018/BTJ_Batteries_AUG2018_FULL.pdf.

[5] L Garten, Heather. “Many unknowns of lithium ion battery safety in Aerospace.” GSTF Journal on Aviation Technology, vol. 1, no. 2, 1 Mar. 2015, https://doi.org/10.5176/2382-5758_1.2.7.

[6] Pandian, G., Pecht, M., Enrico, Z.I.O. and Hodkiewicz, M., 2020. Data-driven reliability analysis of Boeing 787 Dreamliner. Chinese Journal of Aeronautics, 33(7), pp.1969-1979.

[7] Tan, M., Gan, Y., Liang, J., He, L., Li, Y., Song, S. and Shi, Y., 2020. Effect of initial temperature on electrochemical and thermal characteristics of a lithium-ion battery during charging process. Applied Thermal Engineering, 177, p.115500.

[8] “Boeing’s Battery Fix Preserves 787 Systems.” Aviation Week Network, 29 Apr. 2013, aviationweek.com/air-transport/boeings-battery-fix-preserves-787-systems.

[9] Wang, Zengpeng, et al. “Heat transfer characteristics and influencing factors of immersion coupled direct cooling for battery thermal management.” Journal of Energy Storage, vol. 62, June 2023, p. 106821, https://doi.org/10.1016/j.est.2023.106821.

[10] Atyabi, Seyed Ali, et al. “Comparison of active and passive cooling of proton exchange membrane fuel cell using a multiphase model.” Energy Conversion and Management, vol. 268, Sept. 2022, p. 115970, https://doi.org/10.1016/j.enconman.2022.115970.

[11] Van Heerden, A.S., Judt, D.M., Jafari, S., Lawson, C.P., Nikolaidis, T. and Bosak, D., 2022. Aircraft thermal management: Practices, technology, system architectures, future challenges, and opportunities. Progress in Aerospace Sciences, 128, p.100767.

[12] Srivastava, M. and Rathee, S., 2022. Additive manufacturing: Recent trends, applications and future outlooks. Progress in Additive Manufacturing, 7(2), pp.261-287.

[13] Li, M., Du, W., Elwany, A., Pei, Z. and Ma, C., 2020. Metal binder jetting additive manufacturing: a literature review. Journal of Manufacturing Science and Engineering, 142(9), p.090801.

[14] Dahmen, T., et al. “Characterization of channels made by laser powder bed fusion and binder jetting using X-ray CT and image analysis.” Additive Manufacturing, vol. 36, Dec. 2020, p. 101445, https://doi.org/10.1016/j.addma.2020.101445.

[15] Kumar, A.Y., Wang, J., Bai, Y., Huxtable, S.T. and Williams, C.B., 2019. Impacts of process induced porosity on material properties of copper made by binder jetting additive manufacturing. Materials & Design, 182, p.108001.

[16] Kumar, A., Bai, Y., Eklund, A. and Williams, C.B., 2017. Effects of hot isostatic pressing on copper parts fabricated via binder jetting. Procedia Manufacturing, 10, pp.935-944.

[17] Miyanaji, H., Rahman, K.M., Da, M. and Williams, C.B., 2020. Effect of fine powder particles on quality of binder jetting parts. Additive Manufacturing, 36, p.101587.

[18] Zhang, Yanjun, et al. “Effects of channel shape on the cooling performance of hybrid micro-channel and slot-jet module.” International Journal of Heat and Mass Transfer, vol. 113, Oct. 2017, pp. 295–309, https://doi.org/10.1016/j.ijheatmasstransfer.2017.05.092.

[19] Z. M. Razlan, Bin-Abdun, A. B. Shahriman, D. Hazry, W. A. N. Khairunizam, S. Yaacob, S. F. Ahmed, A. T. Hussain, and H. Kamarudin. “The performance of a heat exchanger designed for cooling electric vehicle car battery system by use base fluid and nano-fluid.” *Applied Mechanics and Materials*, vol. 793, 2015, pp. 573–577